2004-06-20

Autostereoscopic 3D display based on micromirror array

Gregory P. Nordin
nordin@byu.edu

C. H. Ahn

H. J. Cho

S. T. Kowel

J. H. Kulick

See next page for additional authors

Original Publication Citation

J. Yan, S. T. Kowel, H. J. Cho, C. H. Ahn, G. P. Nordin, and J. H. Kulick, "Autostereoscopic 3D display based on micromirror array," Appl. Opt. 43(18) pp. 3686-3696 (24)

Autostereoscopic three-dimensional display based on a micromirror array

Jun Yan, Stephen T. Kowel, Hyoung J. Cho, Chong H. Ahn, Gregory P. Nordin, and Jeffrey H. Kulick

A novel approach for three-dimensional (3-D) display systems implemented with a micromirror array was proposed, designed, realized, and tested. The major advantages of this approach include the following: (1) micromirrors are reflective and hence achromatic (panchromatic), (2) a wide variety of displays can be used as image sources, and (3) time multiplexing can be introduced on top of space multiplexing to optimize the viewing zone arrangements. A two-view (left and right) 3-D autostereoscopic display system was first constructed. Left- and right-eye views in the forms of both still and motion 3-D scenes were displayed, and viewers were able to fuse the stereo information. A multiview (two left and two right) 3-D autostereoscopic display system was then simulated.

OCIS codes: 330.1400, 230.3990, 250.3140.

1. Introduction

A real-time, full-color, and wide-viewing-angle three-dimensional (3-D) display has long been a goal of display technology.[1–17] Real-time 3-D display would greatly enhance visualization of magnetic resonance imaging and computed axial tomography images, architectural plans, flight simulation, as well as education and personal entertainment. The development of 3-D display systems has been the subject of substantial research in recent years[18–23] as part of an intense international competition to develop advanced display systems such as 3-D workstations and virtual reality systems.

The human visual system perceives depth through monocular cues, binocular cues, and motion parallax.[22] The relative importance of these visual cues is summarized by Wickens.[22] In binocular cues, only stereoscopic disparity creates a compelling sense of three dimensions. In addition, horizontal motion parallax is important because it enables the look around effect that is so compelling in holograms. Vertical motion parallax, however, can often be eliminated to reduce information content (to save the data rate).[24]

Computer-generated 3-D graphics or real imagery taken by a camera can provide monocular cues. Stereoscopic systems can supply binocular cues. Head tracking and holography can fulfill the motion parallax requirement.

The Integrated Circuit Vision project, conducted by a research group at the University of Alabama in Huntsville and the University of Cincinnati, implements displays delivering a series of stereoscopic images to a viewing region.[25–28] Because an observer would see a particular single pair of stereo images depending on the head position, both stereoscopic disparity and horizontal motion parallax are provided. Such an approach, the partial-pixels architecture, is shown in Fig. 1. Each pixel of the display is divided into eight pairs of partial pixels, which correspond to the appropriate viewing zones. The partial pixels are diffractive elements, which were implemented as arrays of fixed-amplitude gratings etched in chrome on a quartz substrate. Prototype real-time 3-D devices for monochromatic and color displays were demonstrated. The monochromatic display (designed for 630 nm) had a dimension of approximately 1.2 in. $\times$ 0.8 in. (3 cm $\times$ 2 cm) and 16 views, 8 for the left eye and 8 for the right. The color device was designed for three prime colors, 440, 550, and 630 nm. It had

When this research was performed J. Yan (jyan@ececs.uc.edu), S. T. Kowel, H. J. Cho, and C. H. Ahn were with the Department of Electrical and Computer Engineering and Computer Science, University of Cincinnati, Cincinnati, Ohio 45221-0030. H. J. Cho is now with the Department of Mechanical, Materials and Aerospace Engineering, University of Central Florida, Orlando, Florida 32816-2450. G. P. Nordin and J. H. Kulick are with the Department of Electrical and Computer Engineering, University of Alabama in Huntsville, Huntsville, Alabama 35899.

Received 3 October 2003; revised manuscript received 25 March 2004; accepted 25 March 2004.

0003-6935/04/183686-11$15.00/0

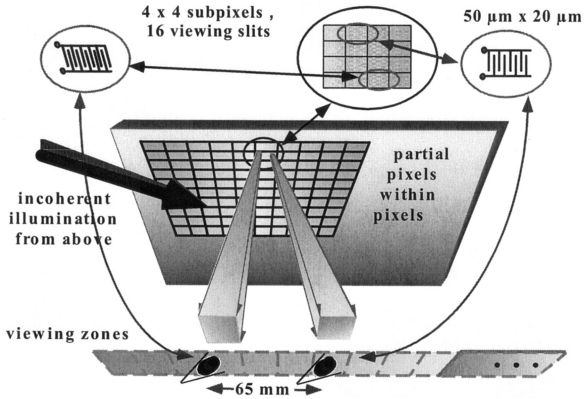

Fig. 1. Three-dimensional display implemented with diffractive partial pixels.

a similar dimension and four views. Both devices produced clearly visible and easily fused 3-D scenes. The color display exhibited vivid color as well.

The major challenge in the development of the diffractive partial-pixel display is how to make a larger screen display and at the same time maintain the color and high resolution. In the partial-pixel prototypes, the spatial light modulator (SLM)—a liquid-crystal display—pixels were spatially multiplexed for eight stereo pairs (16 views). Therefore the resolution was degraded by a factor of 4 in each direction. This is a severe restriction given how difficult it is to increase the pixel count by 16. As an example, a video graphics array (640 × 480) display with 16 views will need $640 \times 480 \times 16 \times 3 \approx 14.7 \times 10^6$ partial pixels, far beyond current capabilities.

In this paper we report on the design, fabrication, and testing of 3-D display systems based on a micromirror array. Figure 2 depicts a conceptual design of the whole system. Two SLMs are used. The first one acts as the image source, on which the time-sequential views are painted. These views are relayed on the second SLM, a micromirror array, which redirects these views into the appropriate viewing zones. Of course the painting of different views (refreshing of the first SLM) and the redirection of the viewing zones (scanning of the micromirrors) should be tightly synchronized.

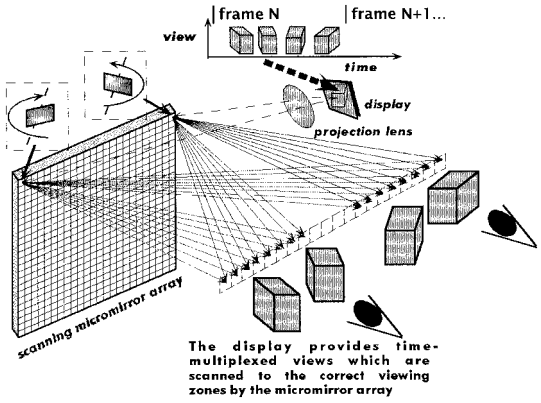

Fig. 2. Direct different 3-D scenes to the corresponding viewing zones by means of time multiplexing.

As an example, let us consider a super video graphics array of 280 μm × 280 μm micromirrors, making up an 8 in. × 6 in. (20 cm × 15 cm) screen. If we supply eight pairs of views, the refreshing rate and scanning speed will be 16 times the normal video refreshing rate, 16 × 60 Hz = 960 Hz. Given the viewing slit size of 6 mm × 10 mm, the normal human interocular distance of 65 mm, and a viewing distance of 300 mm, the scanning range is

$$\theta_{\text{scan}} = \pm\tan^{-1}\left(\frac{65 + 8 \times 6}{2 \times 300}\right) = \pm 10.7^\circ. \qquad (1)$$

These requirements for the scanning of micromirrors are currently feasible. The horizontal size of a viewing slit is designed to be approximately 6 mm, which will just fill the human pupil size. However, the vertical size should be much larger, otherwise it will be difficult for a person to find the views.

The major advantages of this approach include the following: (1) micromirrors are reflective and hence achromatic (panchromatic), (2) a wide variety of displays can be used as image sources, and (3) time multiplexing can be introduced on top of space multiplexing to optimize the viewing zone arrangements.

2. Optical Design for a Microelectromechanical System Three-Dimensional Display

In this section we use an optical ray-tracing program, BeamThree, to design and simulate the 3-D systems. Because the software does not provide ray-tracing options for individual micromirrors, we approximate these with a tilting mirror. If the deflection angle is small, the approximation will be good enough for simulation purposes. We begin with an initial design, which is the most straightforward approach from the optics perspective. The microelectromechanical system (MEMS) design and fabrication was performed in parallel. Facing the MEMS fabrication limitations of our laboratory, we modified our optical design to accommodate the realizable micromirror arrays, as discussed in detail in Section 3.

A. Generic Optical Design for a Microelectromechanical System Three-Dimensional Display

The initial system is the exact approach shown in Fig. 2, where left- and right-eye views are relayed onto the micromirror array and then redirected to the viewing zones. To do so, the micromirrors must be actuated two dimensionally (horizontally and vertically), and the actuations are different depending on the micromirror position. In Fig. 3 a micromirror array is approximated by a titling concaved mirror, which shows the redirection for left and right viewing zones.

The concave radius R is determined by the imaging equation

$$\frac{1}{S_{\text{RLMM}}} + \frac{1}{S_{\text{MMVZ}}} = \frac{1}{-R/2}, \qquad (2)$$

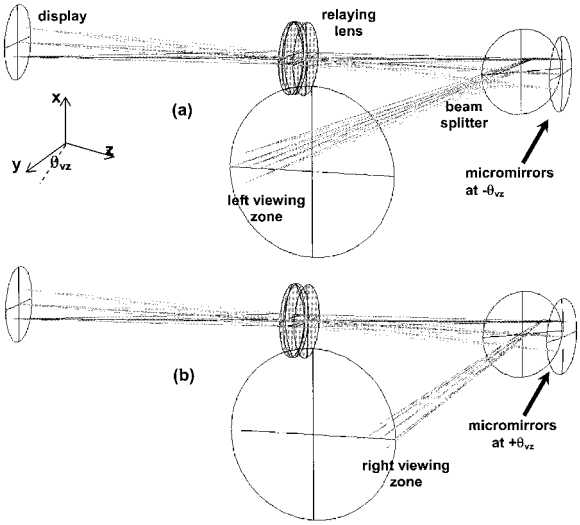

Fig. 3. Initial system: (a) left viewing zone and (b) right viewing zone.

where S_{RLMM} is the distance between the relaying lens and the micromirrors and S_{MMVZ} is the distance between the micromirrors and the viewing zones.

Depending on the micromirrors' position in (x, y), they should have their surface normal pointed to

$$\begin{cases} \alpha = \cos^{-1}[-x/(x^2 + y^2 + R^2)^{1/2}] \\ \beta = \cos^{-1}[-y/(x^2 + y^2 + R^2)^{1/2}] \pm \theta_{\mathrm{vz}} \end{cases}, \quad (3)$$

where $\cos^2\alpha + \cos^2\beta + \cos^2\gamma = 1$; and α, β, and γ are directional angles with respect to the X, Y, and Z axes, respectively (as shown in Fig. 4). θ_{vz} is half of θ_{scan} from Eq. (1) because the scanning angle is twice the deflection angle of a mirror.

The first terms of Eq. (3) make up a spherical contour, and θ_{vz} is for the scanning of horizontal viewing zones. It is quite simple to convert the directional angles to the rotation angles with respect to the X ($\theta_{\mathrm{mm}x}$) and the Y axes ($\theta_{\mathrm{mm}y}$) because $\theta_{\mathrm{mm}x} = \beta - \pi/2$ and $\theta_{\mathrm{mm}y} = \pi/2 - \alpha$.

$$\begin{cases} \theta_{\mathrm{mm}x} = \sin^{-1}[y/(x^2 + y^2 + R^2)^{1/2}] \pm \theta_{\mathrm{vz}} \\ \theta_{\mathrm{mm}y} = -\sin^{-1}[x/(x^2 + y^2 + R^2)^{1/2}] \end{cases}. \quad (4)$$

These are the actuation requirements for micromirrors of our initial system. Although this actuation profile is possible, like the Lucent Technologies WaveStar LambdaRouter,[29] it is complicated for MEMS design, fabrication, and control. Fortunately, we can modify our optical system to simplify the actuation requirements.

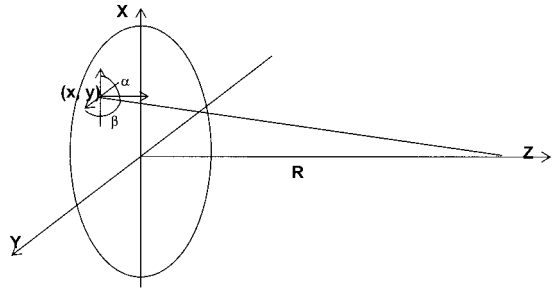

Fig. 4. Directional angles α and β for a spherical contour.

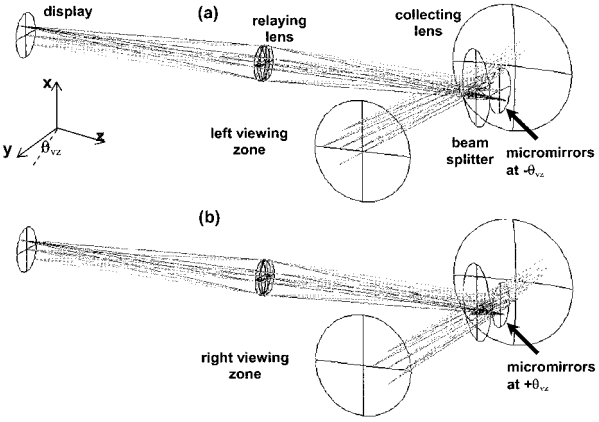

Fig. 5. Optical ray-tracing layout for (a) left viewing zone and (b) right viewing zone. After we introduce the collecting lens, only the uniformly horizontal actuation is required.

B. Collecting Lens for Uniform and Horizontal Actuation

First, another collecting lens is introduced, as shown in Fig. 5, to lower the actuation requirements to be uniformly one dimensional (horizontal). Because the collecting lens will collect light deflected from the micromirrors to form left and right viewing zones, it is functionally equivalent to the spherical contour as shown in Fig. 4. The collecting lens can be either a positive lens or a concave mirror. Practically, a mirror is preferred because it can be made in a larger diameter and it is already achromatic.

Figure 5 shows the optical ray-tracing simulations of a micromirror array with a concave mirror. We can rewrite the actuation requirements as

$$\begin{cases} \theta_{\mathrm{mm}x} = \pm\theta_{\mathrm{vz}} = \pm 5.3^\circ \\ \theta_{\mathrm{mm}y} = 0 \end{cases}, \quad (5)$$

where $\theta_{\mathrm{vz}} = \theta_{\mathrm{scan}}/2$. This is a significant simplification compared with Eq. (4).

C. Interleaving Deflection Profile for Left and Right Viewing Zones

The second simplification takes advantage of the separation between left and right viewing zones as show in Fig. 6(a): There is an unoccupied region between the left eight and right eight viewing zones. Instead of using one micromirror to scan all 16 viewing zones, we can use two micromirror columns, one for the left viewing zones and the other for the right viewing zones. The whole micromirror array will be an interleaved actuation profile as shown in Fig. 6(b).

The introduction of interleaved actuation reduces the requirement of the driving force one step further. As a calculation similar to Eq. (1) shows, the actua-

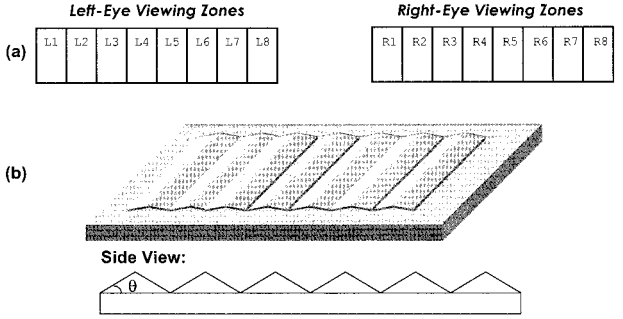

Fig. 6. (a) Left and right viewing zones separation and (b) interleaved micromirror profile for left and right viewing zones.

tion requirement of each micromirror is reduced to $\pm 2.3°$:

$$\theta_{\mathrm{mm}x} = \pm \tan^{-1}\left(\frac{8 \times 6}{2 \times 300}\right)\Big/ 2 = \pm 2.3°. \qquad (6)$$

Because every single frame of the image source provides two views, this actuation profile also lowers the refreshing rate requirements for the image source as discussed in Section 1. For a display with 16 viewing zones, instead of 16 times the standard frame rate, this actuation profile needs only eight times the standard frame rate. Of course, the trade-off is that twice the number of horizontal pixels is required.

D. Double-Opening Pupil at the Relaying Lens

A $\pm 2.3°$ horizontal actuation is quite practical for MEMS design and fabrication. However, we can actually lower the requirement further by introducing a double opening at the relaying lens. This simplification is partially motivated by the fact that the micromirror arrays we fabricated to date have small deflection angles, approximately $\pm 0.8°$, as we discuss in detail in Section 3.

The double-opening pupil approach not only enlarges the viewing zone separation (VZS), but also has the ability to provide more viewing zones. As shown in Fig. 7, for each tilting position of the micromirrors, there are two viewing zones introduced by the double-opening pupil. The separation of the viewing zones is larger than in a single-opening pupil. Hence we can provide left- and right-eye viewing zones even though the physical deflection angles of micromirrors are smaller than the requirements of Eq. (5) or (6).

Furthermore the double-opening pupil can be controlled to be alternative on and off, that is to say, the left opening is on and the right opening is off at the same time, then the left opening is off and the right opening is on. We can actually provide four viewing zones with just two tilting positions of the micromirrors.

Because the double openings are actually out of optical axis, the alignment is strict. The double-opening pupil should be perfectly perpendicular to the optical axis so that the double openings are symmetric and the light is evenly distributed.

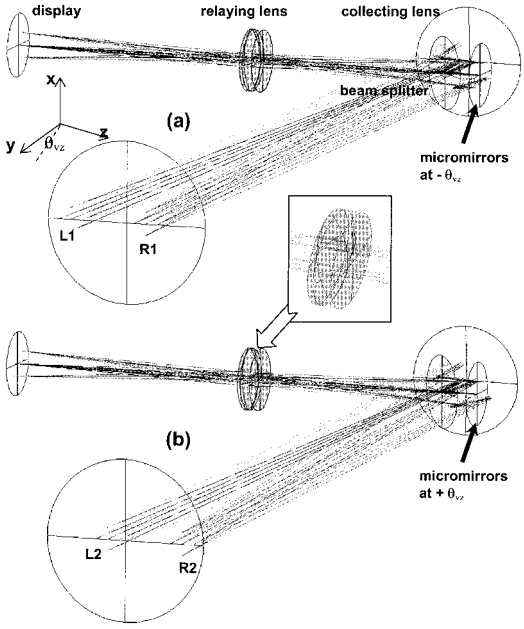

Fig. 7. Optical system design with the double-opening pupil (inset): (a) L1 and R1 viewing zones and (b) L2 and R2 viewing zones.

Finally, we made a detailed analysis on the optical system with a double-opening pupil. Because this is the most complex arrangement of our optical system designs, our analysis includes all features of other systems previously introduced. Figure 8 shows the top view of Fig. 7(a). Only two rays are shown to clarify the drawing.

If the image relay from the display to the micromirror array has a magnification of -1, then the distance between the relaying lens and the micromirror array is $2f_r$. The collecting lens (f_c) has two functions: (a) to form a virtual image of the micromirror array (possible magnification) and (b) to form real images of the relaying lens pupil, which are the viewing zones:

$$\begin{cases} \dfrac{1}{S_1} + \dfrac{1}{S_1'} = \dfrac{1}{f_c} \\ \dfrac{1}{S_2} + \dfrac{1}{S_2'} = \dfrac{1}{f_c} \end{cases}, \qquad (7)$$

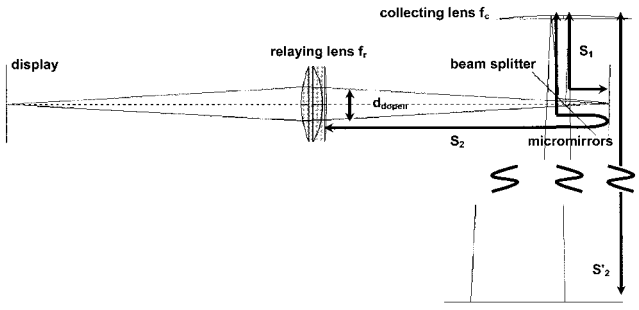

Fig. 8. Optical system analysis.

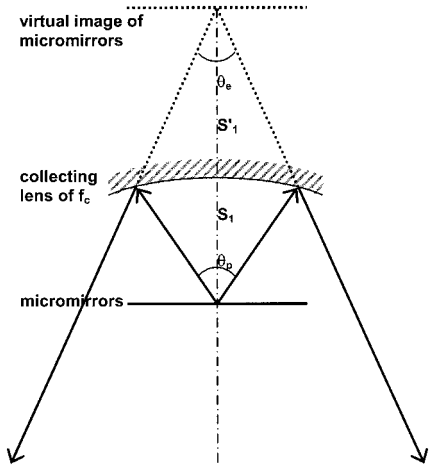

Fig. 9. Geometric arrangement of $(-S_1' + S_2')$, θ_e, and θ_p.

where S_1 is the distance from the micromirror array to the collecting lens and S_2 is the distance from the relaying lens to the collecting lens, as shown in Fig. 8.

The physical scanning range θ_p is the summation of the angles introduced by the double-opening pupil θ_{dopen} and that of the micromirror:

$$\theta_p = \theta_{\text{dopen}} + 2\theta_{\text{mmx}} = 2 \tan^{-1}\left(\frac{d_{\text{dopen}}/2}{2f_r}\right) + 2\theta_{\text{mmx}}, \tag{8}$$

where d_{dopen} is the distance between the two openings of the pupil.

The effective scanning angle θ_e is given by

$$\tan\left(\frac{\theta_e}{2}\right) = \frac{\tan\left(\frac{\theta_p}{2}\right)}{M_2} = \frac{\tan\left(\frac{\theta_p}{2}\right)}{-\frac{S_2'}{S_2}}, \tag{9}$$

where M_2 is the magnification between S_2' and S_2. If θ_p is small, $\theta_p \approx \theta_p/M_2$.

Our goal is to make the viewing zone separation

$$\text{VZS} = (-S_1' + S_2')2 \tan\left(\frac{\theta_e}{2}\right) \tag{10}$$

to be the average human interocular distance of 65 mm, where $(-S_1' + S_2')$ is the effective viewing distance. The geometric arrangement of $(-S_1' + S_2')$, θ_e, and θ_p is shown in Fig. 9. As we show in Section 4, we can achieve this goal even if θ_{mmx} is as small as $\pm 0.8°$.

It is obvious that the more simplified the actuation requirements for micromirrors, the more complicated the optical system. A practical system design will be a careful balance mainly between the optics and the MEMS, although we might consider other system design issues such as the image source refreshing rate. As an example, if a deflection angle of $\pm 5.3°$ is easy to achieve, an optical system like that of Fig. 5 will be sufficient.

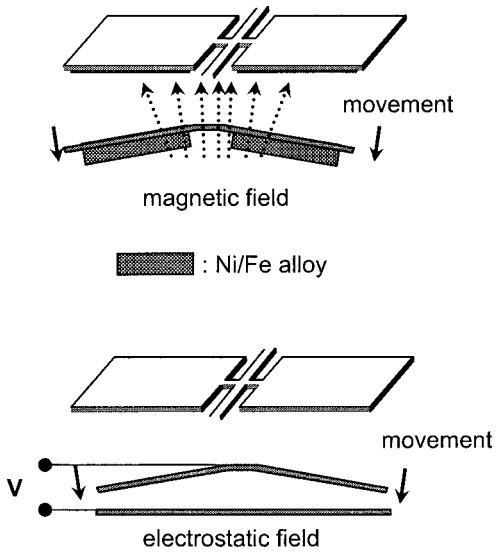

Fig. 10. Electrostatic and magnetic actuation methods.

3. Design, Fabrication, and Testing of Micromirror Arrays

A. Microelectromechanical System Design and Fabrication Processes

The MEMS design was quite straightforward: We first make a membrane and then create hinge and micromirror structures onto the membrane. We had two actuation methods, magnetic and electrostatic, as shown in Fig. 10.

The fabrication steps for magnetic-actuated mi-

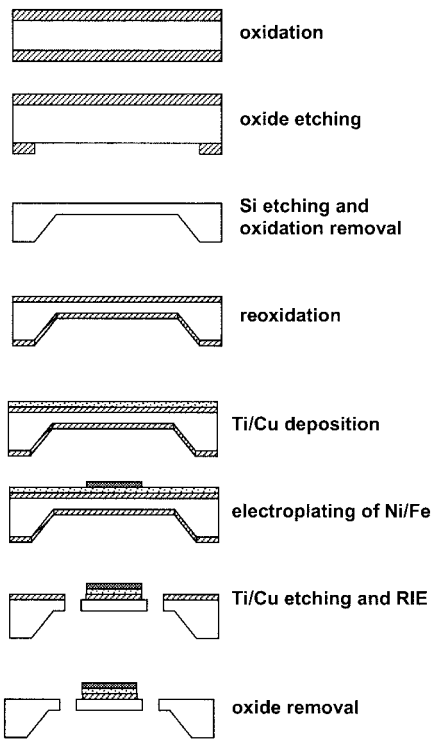

Fig. 11. Fabrication process for magnetic-actuated micromirrors. RIE, reactive ion etching.

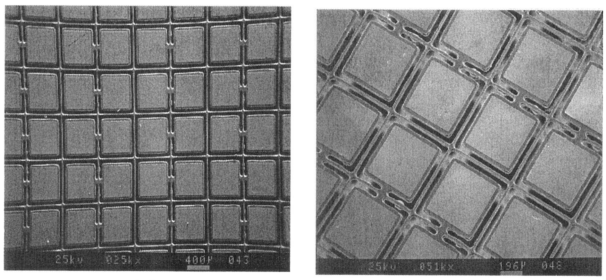

Fig. 12. Fabricated mirror arrays with electroplated Permalloy films: (a) view from the top and (b) view from another angle.

cromirrors are shown in Fig. 11. First, the silicon wafer was oxidized, patterned, and etched to make a 10–20-μm silicon membrane. Second, the wafer was reoxidized, and a metal layer of Ti(200 Å)/Cu(2000 Å) was deposited as a electroplating seed layer. Photoresist was then spun on the wafer and patterned to build the electroplating mold for a Permalloy array. The Permalloy array was electroplated up to the thickness of 8 μm. Third, the micromirrors were patterned and released by reactive ion etching. Finally, the micromirrors were coated with either gold or aluminum to obtain high reflectivity.

The fabrication steps for electrostatic-actuated micromirrors are the same as that of magnetic-actuated micromirrors, except for the electroplating of the Permalloy array. We also keep the metal layer for when we apply the voltage.

B. Fabricated Micromirrors and Discussion

Figure 12 shows scanning electron microscope pictures of a finished micromirror array with a Permalloy layer. The actual dimensions are 403 μm × 403 μm Permalloys and 463 μm × 463 μm micromirrors with a center-to-center distance of 568 μm and a thickness of approximately 20 μm. Electrostatic-actuated micromirror arrays have the same structure without the Permalloy layer. We made several micromirror arrays, with slightly different dimensions.

We used a He–Ne laser as an input and measured the deflected distance at a screen. Although the movements of micromirrors are quite uniform across the array, the actuation angles, denoted by θ_{mmx} in Section 2, are ±0.79° for magnetic actuation and ±0.84° for electrostatic actuation. The major reason for the inflexibility of micromirrors is that their hinges are too thick. We tried to make a hinge thickness down to 5–10 μm, but we did not succeed. A modified fabrication process such as surface micromachining is a possible way to achieve a thinner mirror hinge and thus a larger deflection angle.

4. Testing of the Optical System

A. System Setup

Using backlit transparencies as the image source, we first tested the optical system with a collecting lens

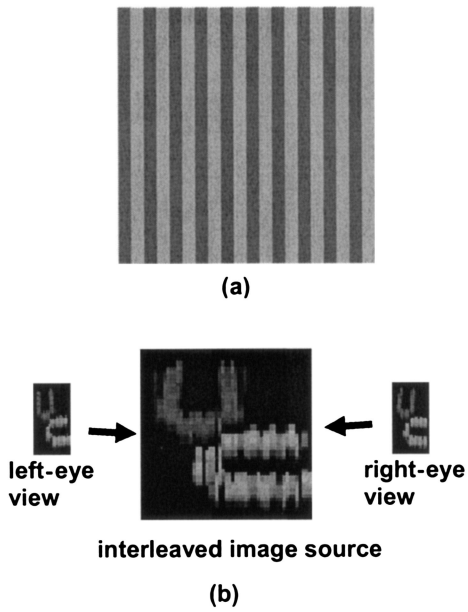

Fig. 13. Image source preparation: (a) color testing and (b) stereo image testing.

(Fig. 5). Figure 13 shows two interleaved pictures for color (magenta and cyan) testing and stereo image testing.

All the parameters for our optical system are listed in Table 1. If we put these numbers, and ±0.8° actuation angles (θ_{mmx}) of the micromirrors, into Eqs. (8)–(10), we can obtain a VZS of 21.8 mm for a single-opening pupil (corresponding to Fig. 5).

The adjustment of the optical system is quite subtle. One actual picture of an almost perfect image relay is shown in Fig. 14, where every pixel of the image source corresponds to a micromirror. This ensures that left- and right-eye pictures will be redirected to the left and right viewing zones.

B. Color Image Testing

The first optical testing was for the separation of the left and right viewing zones. We used a single-opening pupil at the relaying lens. Interleaved cyan and magenta color stripes as shown in Fig. 15(a) were used as our image source, and the system was set up in such a way that the magenta stripes were relayed on the micromirrors for the right viewing zones (odd columns) and the cyan stripes for the left (even columns). We verified these optical ray-tracing simulations experimentally: If the observer moves the eyes, or a camera, from left to right, a clear separation between the cyan and magenta colors is observed as shown in Figs. 15(b) and 15(c), which are actual pictures taken by a camera. Given the geometry, individual micromirrors could not be distinguished. In this case of a single-opening pupil, the separation between left and right viewing zones is 22 mm, which is less than our goal of 65 mm.

Table 1. Optical System Parameters[a]

Subfunction	Lens	Object Distance	Image Distance
Image relay	Relaying lens $f_r = 65$	$2f_r = 130$	$2f_r = 130$
Virtual image of micromirror array	Collecting lens $f_c = 140$	$S_1 = 59$	$S_1' = -102$
Viewing zones	Collecting lens $f_c = 140$	$S_2 = 2f_r + S_1 = 189$	$S_2' = 540$

[a]Units in millimeters; paraxial approximation

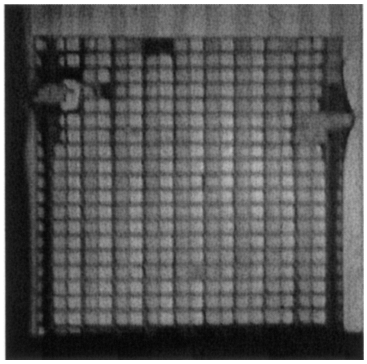

Fig. 14. Actual picture of an almost perfect image relay onto a micromirror array with a one-to-one correspondence between the image source and the micromirror array.

C. Stereoscopic Image Testing

The second optical test is for the stereoscopic image. We used the interleaved stereo picture as shown in Fig. 16(a). The color stripes wrapping around the stereo image are used as references to ensure that the right image is in the odd columns of the micromirrors and the left image is in the even columns.

The left- and right-eye views were observed when we moved our eyes or a camera from the left and right viewing zones. Figures 16(b) and 16(c) show the actual pictures taken by a camera. The stereoscopic disparity between left- and right-eye views is perceivable.

If we had used a larger deflection angle, $\pm 2.3°$ as calculated in Eq. (6), we could have achieved our goal of a 65-mm VZS just using a single-opening pupil. Even with the 22-mm separation, these testing results proved the concept of the use of micromirrors to redirect light for all colors and were important intermediate steps.

5. Prototype Three-Dimensional Display Systems

A. Two-View Autostereoscopic Three-Dimensional Display with a Double-Opening Pupil

As mentioned in Section 2, we trade off a straightforward optical system against simplified actuation requirements for micromirrors. An optical system with the double-opening pupil requires much more

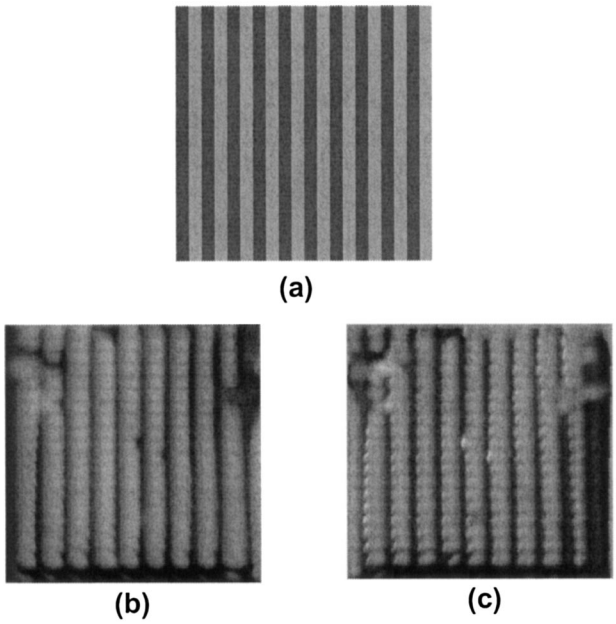

Fig. 15. Color test result for a single-opening pupil: (a) the image source, (b) left image, (c) right image. The left–right separation is 22 mm.

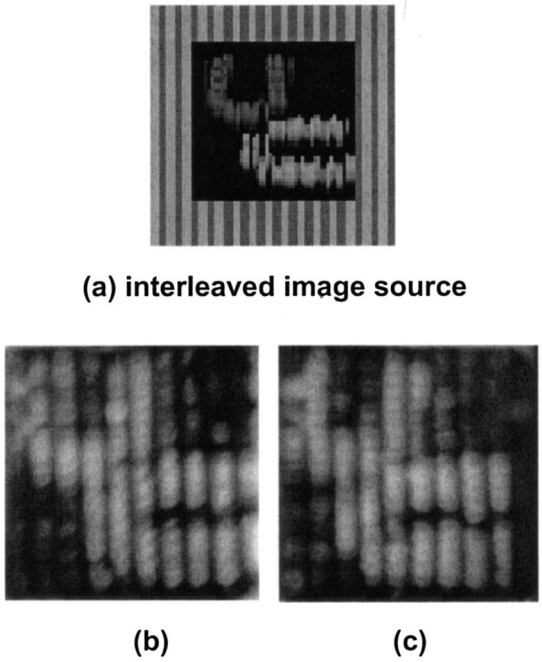

Fig. 16. Stereo image testing result for a single-opening pupil: (a) the image source, (b) left image, (c) right image with a 22-mm separation.

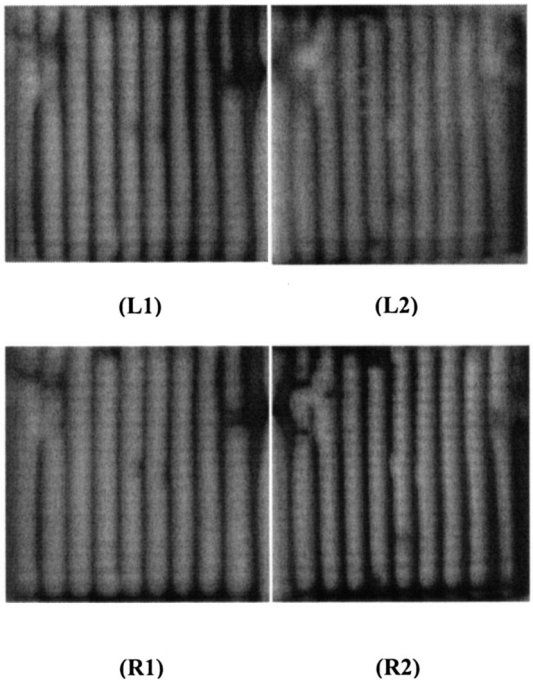

Fig. 17. Color testing result for double-opening pupil. The pictures were taken at the L1, L2, R1, and R2 viewing zones. The separation between L1 and R2 is 66 mm.

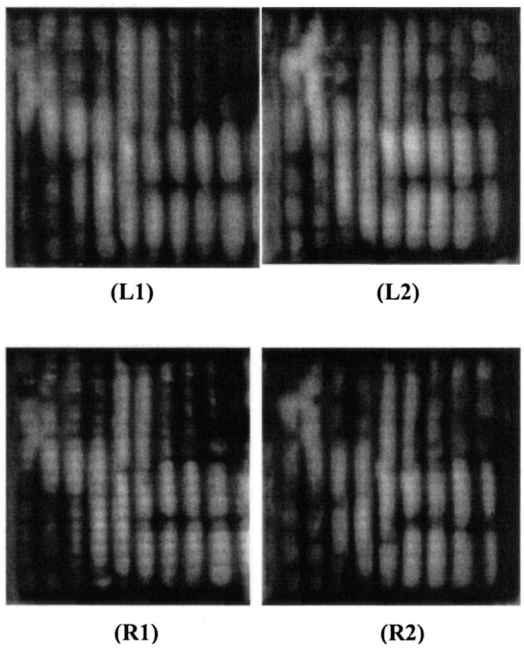

Fig. 18. Stereo image testing result for double-opening pupil. The pictures were taken at the L1, L2, R1, and R2 viewing zones. The separation between L1 and R2 is 66 mm.

accurate adjustment. Because it has two off-axis pupils, every element should be precisely perpendicular to the optical axis. When we use the same optical system listed in Table 1, a 15-mm-apart double-opening pupil, the separation between L1 and R2 viewing zones as shown in Fig. 7 is 64.7 mm, which is close to the average human eye separation of 65 mm.

For color image testing, we used the same image source as show in Fig. 15(a) and set up the system so that the right image is in the odd columns of the micromirrors and the left image is in the even columns. We verified these optical ray-tracing simulations of a double-opening pupil experimentally: If we move our eyes or a camera from left to right, we can observe clearly separated cyan and magenta colors in four positions, which correspond to the viewing zones labeled as L1, L2, R1, and R2 in Fig. 7. Figure 17 shows real pictures taken at these four positions. In this case the picture of L1 is the same as R1, and L2 is the same as R2. The separation between L1 and R2 is 66 mm, which is on target for average human eyes separation.

Because of this separation, if an observer positioned the head correctly (approximately 540 mm from the collecting lens), a cyan picture can be seen from the left eye and a magenta picture from the right eye simultaneously. This is exactly what we designed for an autostereoscopic 3-D display.

For stereoscopic image testing, we used the interleaved stereo pictures as shown in Fig. 16(a) and set up the system so that the right image is in the odd columns of the micromirrors and the left image is in the even columns. Four viewing zones, labeled as L1, L2, R1, and R2, were observed when we moved our eyes or a camera from left to right. Figure 18 shows real pictures taken at these four positions. Again the separation between L1 and R2 is 66 mm, so one can see the left image from the left eye and the right image from the right eye simultaneously. Several people have seen these images and successfully fused the images. To our knowledge this was the first demonstration of an autostereoscopic 3-D display system by use of a micromirror array to direct light to viewing zones.

One step further, we used an ordinary color cathode-ray tube (CRT) as the image source so that we could update the image source dynamically. The image source preparation is also similar to that of the testing system. For an image relay from the image source to the micromirror array with a magnification of -1, and odd (even) columns of the micromirrors pointing to the right (left) viewing zone, the image source should be an interleaving between left and right views. To match the micromirror separation of 568 μm $\times$ 568 μm with the 0.28-mm dot pitch of the color CRT, we simply used a block of 2×2 CRT pixels to make up one image source pixel. An example image source is shown in Fig. 19, in which the picture is flipped for -1 magnification and wrapped with red and green stripes for reference.

An observer can see the left image with the left eye and the right image with the right eye. Because in this case L1 is the same as R1, and L2 is the same as R2, only pictures taken at L1 and R2 are shown in Fig. 20. Note that the white signals are actually a combination of red, green, and blue phosphors, so the

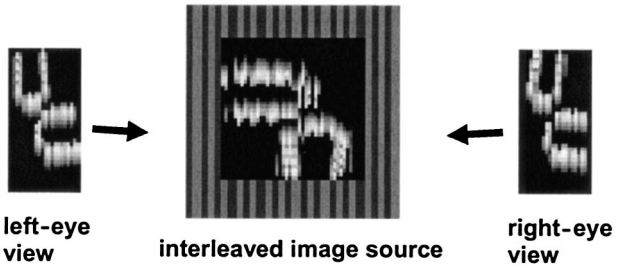

Fig. 19. Example image source on the color CRT.

pictures again proved that our system worked for all colors.

We can now call our system a prototype 3-D display because it is a full-color and real-time system. We have displayed several 3-D still pictures and animations on our prototype system, which were viewed successfully by members of our group.

B. Simulation of Multiple-View Autostereoscopic Three-Dimensional Display

We already have four viewing zones, L1, L2, R1, and R2; but what we see from L1 is the same as R1, and L2 is the same as R2. We propose to use an alternative shutter for the double-opening pupil; and if the shutter is synchronized with the CRT, we can actually provide four different viewing zones.

The system has two more gradual modifications on top of the two-view prototype. The first modification is an alternative shutter for the double-opening pupil, as shown in Fig. 21. For the relaying lens, the pupil at the $+y$ position is opened and the other is closed at time $2mt_0 + 1$; then the pupil at the $-y$ position is opened and the other is closed at time $2mt_0$, where t_0 is the open duration of one pupil and $m = 0, 1, 2, \ldots$. This pupil shutter can be easily realized with a liquid-crystal shutter.

The second modification is a dynamically changing image source synchronized with the alternative shutter at the double-opening pupil, as shown in Fig. 22. At time $2mt_0 + 1$, an interleaved image of the L1 and L2 views is displayed; and then the interleaved image of the R1 and R2 views is displayed at time $2mt_0$. At time $2mt_0 + 1$, view L1 will be relayed onto an even column of the micromirrors and redirected to viewing zone L1; view L2 will be relayed onto an odd column

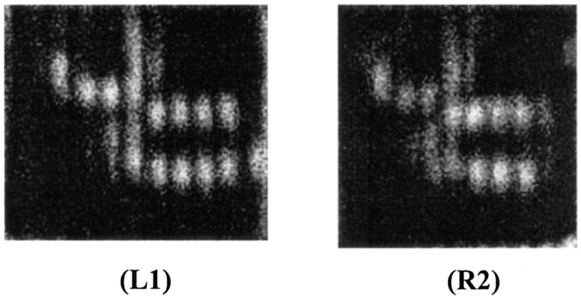

Fig. 20. Pictures taken from the left (L1) and right (R2) viewing zones, which are 66 mm apart.

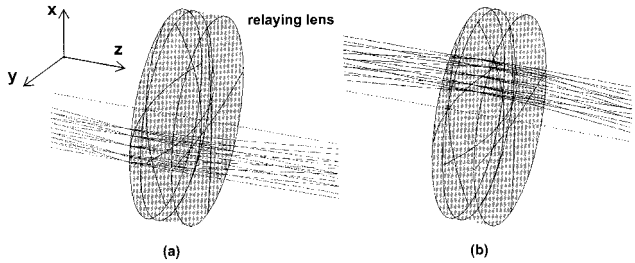

Fig. 21. Alternatively opened and closed double-opening pupil at the relaying lens: (a) pupil at the $+y$ position is open at time $2mt_0 + 1$ and (b) pupil at the $-y$ position is open at time $2mt_0$.

of the micromirrors and redirected to viewing zone L2. Similar relaying and redirecting for R1 and R2 will be performed at time $2mt_0$. If t_0 is small enough so that the L1, L2, R1, and R2 views seem to appear simultaneously, we can provide multiview autostereoscopic 3-D scenes.

The optical system parameters are the same as listed in Table 1. The only difference is a 23-mm-apart double-opening pupil. A calculation with Eqs. (8)–(10) shows that separation between the L1 and R1 viewing zones is 65.6 mm, and the separation between L1 and L2 is 21.8 mm. An optical ray tracing as shown in Fig. 23 gave the result of 66 and 22 mm of separation from L1 to R1 and L1 to L2, respectively. In this configuration, an observer would see L1 from the left eye and R1 from the right eye and fuse the images. If the observer moves slightly to the right (approximately 22 mm), L2 would be seen from the left eye and R2 from the right eye and form another 3-D perspective. Therefore both stereoscopy and horizontal motion parallax would be provided.

Although the L1–R1 and L2–R2 separations are

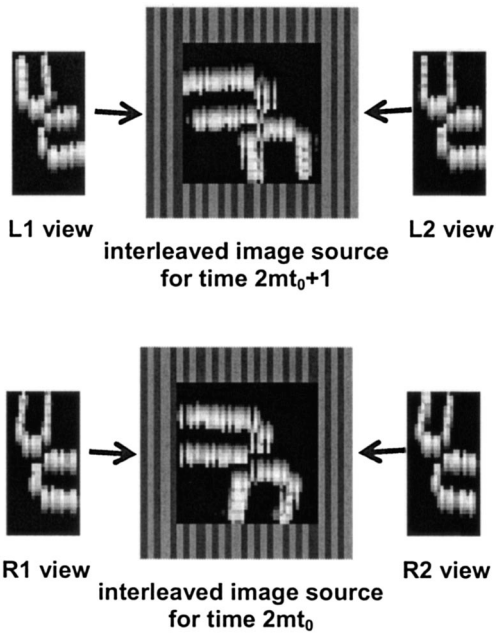

Fig. 22. Example image source sequence on the color CRT.

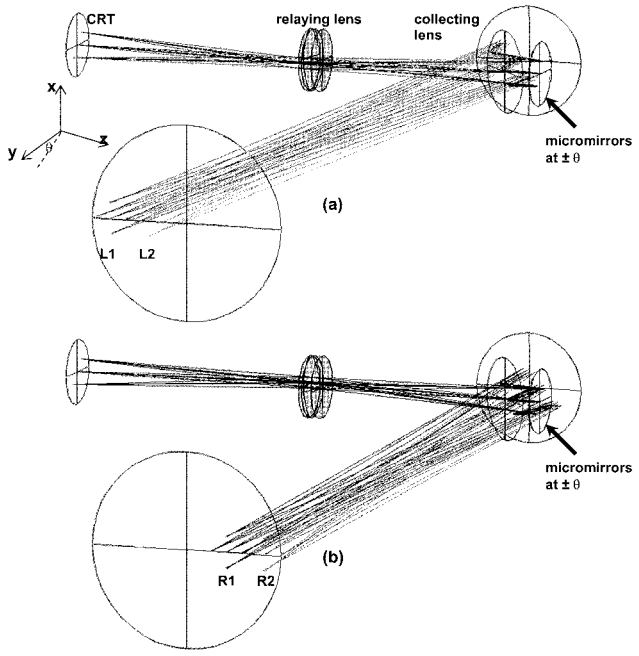

Fig. 23. Optical ray tracing for the multiview (two left and two right) 3-D display: (a) at time $2mt_0 + 1$, interleaved L1 and L2 views are displayed, pupil at the $+y$ position is open; (b) at time $2mt_0$, interleaved R1 and R2 views are displayed, pupil at the $-y$ position is open.

appropriate for human eye separation, the distances between L1–L2 and R1–R2 are not optimal. The later distances should be 6 mm, which is the average human pupil size, so that the provided motion parallax could be close to the real-world 3-D viewing experience. We could not fulfill this criterion because we had to tune the system to reach our main goal—the 65-mm binocular separation.

We have not obtained any experimental results for the multiview 3-D system so far, partially because of the difficulty of the optical system adjustment. However, the simulation shows one way of providing multiple views.

6. Conclusion

We proposed a novel approach for 3-D display systems implemented with a micromirror array. The major advantages of this approach include the following: (1) micromirrors are reflective and hence achromatic (panchromatic), (2) a wide variety of displays can be used as image sources, and (3) time multiplexing can be introduced on top of space multiplexing to optimize the viewing zone arrangements.

We analyzed our proposal in detail and calculated the requirements for micromirror actuations. Then we fabricated the first micromirror arrays for the 3-D display, although the achieved actuation degree ($\pm 0.8°$) was not big enough for our design. In a concurrent optics design, we introduced three modifications in the system design: (1) a collecting lens, (2) an interleaved actuation profile, and (3) a double-opening pupil to accommodate the fabricated micromirror array.

A two-view (left and right) 3-D autostereoscopic display system was first constructed. Left- and right-eye views in the form of both still and motion 3-D scenes were displayed, and viewers were able to fuse the stereo information. A multiview (two left and two right) 3-D autostereoscopic display system was also proposed. We alternatively switched two slits of the double-opening pupil on and off and synchronized the switch with the CRT. At one time frame, L1 and L2 views can be provided. At the following time frame, R1 and R2 views can be provided. The distance from L1 to R1 was 66 mm and from L1 to L2 it was 22 mm.

We believe that these results marked a promising step toward a personal multiview autostereoscopic 3-D display system. However, we were still facing many technical difficulties, the major one being the small deflection angles of micromirrors, which limited our design and realization of prototype systems. Further improvements include micromirrors with larger deflection angles and dynamic control, systems with a bigger display area and higher resolution, and systems with more viewing zones for better motion parallax presentation.

This study was partially supported by National Science Foundation Experimental Program to Stimulate Competitive Research EPS-9720653; it was also supported by the University of Cincinnati.

To avoid the high cost of color printing, this paper is converted to black-and-white format. We will keep a color version of this paper at http://www.eng.uc.edu/~skowel/. We also previously published a much shorter paper with intermediate results in color.[30]

References

1. R. D. Ketchpel, "Direct view three dimensional display tube," IEEE Trans. Electron. Devices **ED-10,** 324–328 (1963).
2. E. G. Rawson, "Vibrating varifocal mirrors for 3D imaging," IEEE Spectrum **6,** 37–43 (1969).
3. M. C. King and D. H. Berry, "Varifocal mirror technique for video transmission of 3-D images," Appl. Opt. **9,** 2035–2039 (1970).
4. H. Bartelt and N. Streibl, "Three dimensional display based on thick holographic phase components," Opt. Eng. **24,** 1038–1041 (1985).
5. A. A. Adumbrate, E. Abel, and S. Murphy, "3-D TV system for remote handling: development and evaluation," in *Stereoscopic Displays and Applications*, S. S. Fisher and J. O. Merritt, eds., Proc. SPIE **1256,** 226–236 (1990).
6. A. R. Travis, "Autostereoscopic 3-D display," Appl. Opt. **29,** 4341–4342 (1990).
7. R. Duchowicz, M. Trivi, L. Scaffardi, and N. Bolognini, "Speckle stereograms of moving objects," Appl. Opt. **29,** 1871–1872 (1990).
8. A. P. Maturing, E. R. Jones, Jr., and J. L. Mason, Jr., "3-D endoscopy through alternating-frame technology," in *Stereoscopic Displays and Applications*, S. S. Fisher and J. O. Merritt, eds., Proc. SPIE **1256,** 307–311 (1990).
9. K. E. Joachimowicz and R. S. Gold, "Stereoscopic (3-D) projection display using polarized color," Opt. Eng. **29,** 838–842 (1990).
10. S. Takahashi, T. Toda, and F. Iwata, "Three dimensional grat-

ing images," in *Practical Holography V*, S. A. Benton, ed., Proc. SPIE **1461,** 199–205 (1991).
11. D. R. Wuest and R. S. Lakes, "Holographic optical element for projection of stereo images," Appl. Opt. **31,** 1008–1009 (1992).
12. D. Drascic and J. J. Grodski, "Using stereoscopic video for defense teleoperation," in *Stereoscopic Displays and Applications IV*, J. O. Merritt and S. S. Fisher, eds., Proc. SPIE **1915,** 58–59 (1993).
13. J. B. Eichenlaub, "Developments in autostereoscopic technology at Dimension Technologies Inc.," in *Stereoscopic Displays and Applications IV*, J. O. Merritt and S. S. Fisher, eds., Proc. SPIE **1915,** 177–186 (1993).
14. L. Onural, G. Bozdagi, and A. Atalar, "New high-resolution display device for holographic three-dimensional video: principles and simulations," Opt. Eng. **33,** 835–844 (1994).
15. N. Tetsutani, K. Omura, and F. Kishino, "Wide-screen autostereoscopic display system employing head-position tracking," Opt. Eng. **33,** 3690–3697 (1994).
16. T. Toda, S. Takahashi, and F. Iwata, "Three-dimensional (3D) video system using grating image," in *Practical Holography IX*, S. A. Benton, ed., Proc. SPIE **2406,** 191–198 (1995).
17. M. Shires, "Real-time flat panel solid state holographic stereogram," in *Fifth International Symposium on Display Holography*, T. H. Jeong, ed., Proc. SPIE **2333,** 381–392 (1995).
18. S. A. Benton and J. S. Kollin, "Three-dimensional display system," U.S. patent 5,172,251 (15 December 1992).
19. S. Chen and M. R. Chatterjee, "Implementation of a spatially multiplexed pixelated three-dimensional display by use of a holographic optical element array," Appl. Opt. **37,** 7504–7513 (1998).
20. E. Downing, L. Hesselink, J. Ralston, and R. Macfarlane, "A three-color, solid-state, three-dimensional display," Science **273,** 1185–1189 (1996).
21. C. Penciu and D. L. MacFarlane, "Fabrication and characterization of a volumetric three-dimensional display using ion-exchanged integrated waveguides," Opt. Eng. **39,** 565–571 (2000).
22. C. D. Wickens, "Three-dimensional stereoscopic display implementation: guidelines derived from human visual capabilities," in *Stereoscopic Displays and Applications*, S. S. Fisher and J. O. Merritt, eds., Proc. SPIE **1256,** 2–11 (1990).
23. M. Ziegler, L. Falkenhagen, R. ter Horst, and D. Kalivas, "Evolution of stereoscopic and three-dimensional video," Signal Process. **14,** 173–194 (1998).
24. S. A. Benton, "Survey of holographic stereograms," in *Processing and Display of Three-Dimensional Data*, J. J. Pearson, ed., Proc. SPIE **367,** 15–19 (1982).
25. M. W. Jones, "Partial pixels: a real-time 3-D display architecture," Ph.D. dissertation (University of Alabama in Huntsville, Huntsville, Ala., 1996).
26. M. W. Jones, G. P. Nordin, J. H. Kulick, R. G. Lindquist, and S. T. Kowel, "Real-time three-dimensional display based on the partial pixel architecture," Opt. Lett. **20,** 1418–1420 (1995).
27. J. H. Kulick, G. P. Nordin, A. Parker, S. T. Kowel, R. G. Lindquist, M. W. Jones, and P. Nasiatka, "Partial pixels: a three-dimensional diffractive display architecture," J. Opt. Soc. Am. A **12,** 73–83 (1995).
28. G. P. Nordin, M. W. Jones, J. H. Kulick, R. G. Lindquist, and S. T. Kowel, "Three-dimensional display utilizing a diffractive optical element and an active matrix liquid crystal display," Opt. Eng. **35,** 3404–3412 (1996).
29. V. A. Aksyuk, F. Pardo, C. A. Bolle, S. Arney, C. R. Giles, and D. J. Bishop, "Lucent microstar micromirror array technology for large optical crossconnects," in *MOEMS and Miniaturized Systems*, M. E. Motamedi and R. Goering, eds., Proc. SPIE **4178,** 320–324 (2000).
30. J. Yan, S. T. Kowel, H. J. Cho, and C. H. Ahn, "Real-time full-color three-dimensional display with a micromirror array," Opt. Lett. **26,** 1075–1077 (2001).